Robust Control Design for the FLEXOP Demonstrator Aircraft via Tensor Product Models

Béla Takarics, Bálint Vanek

Systems and Control Lab, Institute for Computer Science and Control, 1111 Budapest, Kende u. 13-17., Hungary

Abstract

The paper proposes a control design methodology for active flutter suppression for the aeroservoelastic (ASE) aircraft of the European project FLEXOP. The aim of the controller is to robustly stabilize the aeroelastic modes. The control design is based on a control oriented linear parameter-varying (LPV) model, which is derived via "bottom-up" modeling approach and includes the parametric uncertainties of the flutter modes. The tensor product (TP) type LPV model is generated via TP model transformation. The symmetric and asymmetric flutter modes are decoupled, which allows independent control design for each. LPV observer based state feedback control structure is applied with constrains on the maximal control value to avoid input saturation. The scheduling parameters of the TP type LPV models are split into measured and uncertain parameters for robust control design. Convex hull manipulation based optimization and model complexity effects are investigated. The resulting controller is validated via the high-fidelity ASE model of the FLEXOP aircraft.

1 Introduction

Future aircraft designs increasingly focus on fuel consumption reduction. This can be achieved by reducing the weight and structure of the aircraft and by increasing its wingspan. Such aircraft have more flexible structures and increased aeroservoelastic (ASE) effects. This manifests in aeroelastic flutter, which is the interaction between the structural dynamics and aerodynamics producing unstable oscillations [12]. Control based active flutter suppression is investigated in several recent research projects. These are the Performance Adaptive Aeroelastic Wing (PAAW) project in the USA [18] and the Flutter Free FLight Envelope eXpansion for ecOnomical Performance improvement (FLEXOP) and Flight Phase Adaptive Aero-Servo-Elastic Aircraft Design Methods (FLiPASED) projects in the EU [10, 11], which are the subject of this paper. A demonstrator Unmanned Areal Vehicle (UAV) is developed in FLEXOP (Section 3.1) and is shown in Figure 1. The flutter

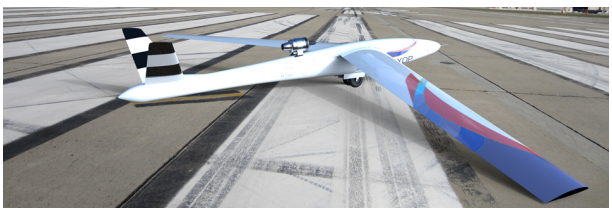

Figure 1: FLEXOP demonstrator aircraft.

suppression controller can be synthesized using an appropriate control oriented model [33, 16, 23]. The ASE

model of an aircraft is the integration of aerodynamics, structural dynamics and flight dynamics subsystems [13, 17], (Section 3.2). The details of the ASE model development of the FLEXOP demonstrator are given in [39, 17]. The aerodynamics model is based on the vortex lattice method (VLM) and doublet lattice method (DLM). The structural dynamics model is obtained from a `Nastran` based finite element (FE) model. The integration of the subsystems relies on the mean axis reference frame [22]. The resulting model consists of 12 rigid body states, 100 states of the structural dynamics and 1040 aerodynamic lag states in addition to the actuator dynamics states. This ASE model of the FLEXOP aircraft is considered as the nominal, high-fidelity model. Control design for such a high dimensional, nonlinear model is challenging. The linear parameter-varying (LPV) framework [24] (Section 2) can be applied instead of the nonlinear model. There are two possible ways to obtain low order LPV models: LPV model order reduction [35, 15] and "bottom-up" modeling [31, 17], which is applied in the paper (Section 3.3). The key idea is the following. The subsystems have simpler structure than the nonlinear ASE model. Therefore, the structural dynamics and aerodynamics models can be reduced by tractable reduction techniques. These reduced order subsystems form a low order nonlinear ASE model upon which the control oriented LPV model can be obtained. The structural dynamics has uncertain parameters that affect the flutter modes. These uncertainties are included in the uncertain control oriented model (Section 3.4).

Three main LPV system representations exist. These are the "grid-based" [38], the linear fractional transformation (LFT) [19] and polytopic [1] LPV systems. The paper focuses on polytopic LPV systems, specifically Tensor Product (TP) polytopic models obtained via TP model transformation [6]. TP model transformation is a numerical tool based on the higher-order singular value decomposition (HOSVD) [9] and it can generate various types of convex polytopic forms [40, 2] for convex hull manipulation based optimization [28, 26]. In addition, the higher-order singular values give a possibility for trade-off between the accuracy and complexity of the resulting model. TP model applications are given in [7, 8, 5, 3, 4].

The main goal of the paper is to propose a TP model based robust control design methodology for active flutter suppression of the FLEXOP aircraft. First, a "bottom-up" model is derived. Second, an uncertain control oriented TP type polytopic model is obtained. Third, the TP model of the FLEXOP aircraft is not an exact representation, therefore balancing between the accuracy and complexity of the TP model is addressed. Fourth, convex hull manipulation based control optimization is investigated. An important benefit of the presented control design is the separation of scheduling and uncertain parameters. Such approach is difficult to apply for grid-based LPV systems. The proposed control structure for the flutter suppression is LPV observer and state feedback design with constraints on the control signal to avoid actuator saturation (Section 4). The controller is validated by frequency domain analysis (Section 4.3) and by time domain simulations with the uncertain high-fidelity, nonlinear model (Section 4.4), followed by the conclusions (Section 5). It is crucial to emphasize that while this paper focuses on flutter suppression control design, the presented control design methodology can be used for a wide class of control applications.

2 LPV Modeling and Control

The following section presents the main concepts of LPV modeling and control design [9, 32, 38, 6].

2.1 Grid-based and polytopic LPV models

An LPV system is described by the state space model [38, 24]

$$\begin{aligned} \dot{x}(t) &= A(\rho(t))\, x(t) + B(\rho(t))\, u(t) \\ y(t) &= C(\rho(t))\, x(t) + D(\rho(t))\, u(t) \end{aligned} \tag{1}$$

with the continuous matrix functions $A\colon \mathcal{P} \to \mathbb{R}^{n_x \times n_x}$, $B\colon \mathcal{P} \to \mathbb{R}^{n_x \times n_u}$, $C\colon \mathcal{P} \to \mathbb{R}^{n_y \times n_x}$, $D\colon \mathcal{P} \to \mathbb{R}^{n_y \times n_u}$, the state $x\colon \mathbb{R} \to \mathbb{R}^{n_x}$, output $y\colon \mathbb{R} \to \mathbb{R}^{n_y}$ input $u\colon \mathbb{R} \to \mathbb{R}^{n_u}$, and a time-varying scheduling signal $\rho\colon \mathbb{R} \to \mathcal{P}$,

where $\mathcal{P}$ is a compact subset of $\mathbb{R}^N$. The system matrix $S(\rho(t))$ is

$$S(\rho(t)) = \begin{bmatrix} A(\rho(t)) & B(\rho(t)) \\ C(\rho(t)) & D(\rho(t)) \end{bmatrix}. \tag{2}$$

In grid-based LPV representation [38], the system is described as a collection of LTI models (A_k, B_k, C_k, D_k) $= (A(\rho_k), B(\rho_k), C(\rho_k), D(\rho_k))$ obtained from evaluating the LPV model at a finite number of parameter values $\{\rho_k\}_1^{n_{\text{grid}}} = \mathcal{P}_{\text{grid}} \subset \mathcal{P}$. In polytopic representation [1]

$$S(\rho(t)) = \sum_{r=1}^{R} w_r(\rho(t)) S_r. \tag{3}$$

$S(\rho(t))$ is defined as the parameter varying combinations of LTI vertex system matrices $S_r \in \mathbb{R}^{(n_x+n_u)\times(n_x+n_y)}$ and weighting functions $w_r(\rho(t))$. Explicit dependence on time t is suppressed in trivial cases in the remainder of the paper.

2.2 TP type polytopic models

The backbone of TP models is the HOSVD [9, 6], the SVD for N-th-order tensors with the notation $\mathcal{X} \overset{N}{\underset{n=1}{\boxtimes}} \mathbf{U}_n$. The core tensor $\mathcal{X}$ contains linear time-invariant (LTI) matrices. The TP type polytopic HOSVD-based canonical model of (3) takes the following structure [25]:

$$S(\rho(t)) = \sum_{i_1=1}^{I_1} \cdots \sum_{i_N=1}^{I_N} \prod_{n=1}^{N} w_{n,i_n}(\rho_n(t)) S_{i_1,\ldots,i_N}. \tag{4}$$

The TP type polytopic form consists of the LTI vertex systems $S \in \mathbb{R}^{(n_x+n_u)\times(n_x+n_y)}$ and the uni-variate weighting functions $w_n(\rho_n(t))$. The compact tensor notation of (4) is

$$S(\rho(t)) = \mathcal{S} \overset{N}{\underset{n=1}{\boxtimes}} w_n(\rho_n(t)). \tag{5}$$

The row vectors $w_n(\rho_n(t))$ are constructed from the univariate weighting functions $w_{n,i_n}(\rho_n(t))$, $i_n = 1 \ldots I_N$, the core tensor $\mathcal{S} \in \mathbb{R}^{I_1\times\ldots\times I_N\times(n_x+n_u)\times(n_x+n_y)}$ from the LTI vertex matrices $S_{i_1,\ldots,i_N}$ and ρ_n is the n-th element of vector ρ.

Definition 1 (Finite element TP type polytopic model) *The LPV model (1) can be defined as a polytopic model using a TP model structure as*

$$\begin{bmatrix} \dot{x}(t) \\ y(t) \end{bmatrix} = \mathcal{S} \overset{N}{\underset{n=1}{\boxtimes}} w_n(\rho_n(t)) \begin{bmatrix} x(t) \\ u(t) \end{bmatrix}. \tag{6}$$

The N+2-dimensional core tensor $\mathcal{S} \in \mathbb{R}^{I_1\times\cdots\times I_N\times(n_x+n_u)\times(n_x+n_y)}$ contains the LTI system matrices $S_{i_1,\ldots,i_N} \in \mathbb{R}^{(n_x+n_u)\times(n_x+n_y)}$.

Definition 2 (Convex TP type polytopic model) *The TP type polytopic model (6) is convex if the weighting functions $w_n(\rho_n(t))$ satisfy the following criteria:*

$$\begin{aligned} &\forall n, \rho_n(t) : \sum_{i=1}^{I_n} w_{n,i}(\rho_n(t)) = 1 \\ &\forall n, i, \rho_n(t) : w_{n,i}(\rho_n(t)) \in [0,1] \end{aligned} \tag{7}$$

The convex representation of the given LPV system is not unique and the specific representation significantly influences the resulting control performance [27, 28]. The following convex hulls are investigated in the paper: CNO (Close to Normal) is a tight convex hull, IRNO (Inverted and Relaxed Normal) is a large convex hull and SNNN (Sum Normalized Non-Negative) that only satisfies the convexity criteria [6]. Convex TP type models can be obtained from the LPV model of (1) via TP model transformation [6]. Assume that the HOSVD of the LPV system of (1) is given and the n-mode rank of $S(\rho)$ is R_n $(1 \leq n \leq n_\rho)$ [6]. The approximate TP type model $\hat{S}(\rho)$ is obtained by discarding small singular values $\sigma^{(n)}_{I'_n+1}, \sigma^{(n)}_{I'_n+2}, \dots \sigma^{(n)}_{R_n}$ of tensor $\mathcal{S}$ for a given $I'_n < R_n$. The upper bound of the approximation error is then

$$\frac{1}{\gamma_{TP}} = \|S(\rho) - \hat{S}(\rho)\|^2 \leq \sum_{i_1=I'_{1+1}}^{R_1} \left(\sigma^{(1)}_{i_1}\right)^2 + \dots + \sum_{i_{n_\rho}=I'_{n_\rho+1}}^{R_{n_\rho}} \left(\sigma^{(n_\rho)}_{i_{n_\rho}}\right)^2. \tag{8}$$

2.3 Control design with TP models

The proposed TP model based control design is done via observer based state feedback, where the observer needs to satisfy the convergence $x(t) - \hat{x}(t) \to 0 \quad \text{as} \quad t \to \infty$, [6, 32]. Both the state feedback controller and the observer are LPV systems that are scheduled by the parameter vector ρ and the control structure is given as

$$\begin{aligned} \begin{bmatrix} \dot{\hat{x}}(t) \\ \hat{y}(t) \end{bmatrix} &= S(\rho(t)) \begin{bmatrix} \hat{x}(t) \\ u(t) \end{bmatrix} + \begin{bmatrix} K(\rho(t)) \\ 0 \end{bmatrix} (y(t) - \hat{y}(t)), \\ u(t) &= -F(\rho(t))\hat{x}(t). \end{aligned} \tag{9}$$

Using the TP type polytopic representation the control design elements, the LPV model $S(\rho(t))$, the controller $F(\rho(t))$ and the observer gain $K(\rho(t))$ have the following form:

$$\begin{aligned} S(\rho(t)) &= \mathcal{S} \bigotimes_{n=1}^{N} w_n(\rho_n(t)), \\ F(\rho(t)) &= \mathcal{F} \bigotimes_{n=1}^{N} w_n(\rho_n(t)), \\ K(\rho(t)) &= \mathcal{K} \bigotimes_{n=1}^{N} w_n(\rho_n(t)). \end{aligned} \tag{10}$$

Such control structure, where the state feedback and observer gains take the same polytopic structure as the LPV model, is known as the parallel distributed compensation (PDC) [32].

2.3.1 LMI based control design

The aim of the control synthesis is to find the state feedback gains $F_{i_1,\, i_2,\, \dots,\, i_N}$ in core tensor $\mathcal{F}$ and observer gains $K_{i_1,\, i_2,\, \dots,\, i_N}$ in core tensor $\mathcal{K}$. Such control synthesis problem can be efficiently solved by LMI techniques. In case of polytopic LPV models the LMIs can be applied directly for the vertex systems $S_{i_1,\, i_2,\, \dots,\, i_N}$ of $\mathcal{S}$ and the corresponding state feedback and observer gains can be obtained.

Theorem 1 Globally asymptotically stable control synthesis: *Consider the TP type polytopic model state feedback controller in the form of (9). The control structure is globally and asymptotically stable if matrices $X = X^T > 0$ and M_r ($r = 1, \dots$ and R denotes the number of LTI vertex systems of (5) satisfy the following inequalities*

$$\begin{aligned} &XA_r^T - M_r^T B_r^T + A_r X - B_r M_r < 0, \\ &XA_r^T - M_s^T B_r^T + A_s X - B_r M_s + XA_s^T \\ &- M_r^T B_s^T + A_s X - B_s M_r < 0 \end{aligned}$$

for $r < s \leq R$, except the pairs (r, s), such that $\forall \rho(t) : w_r(\rho(t))w_s(\rho(t)) = 0$, and where $M_r = F_r X$. The state feedback gains can be obtained as $F_r = M_r X^{-1}$.

Theorem 2 Constraint on the control value: *Assume that the upper bound of the initial condition is known and it is given by $\|x(0)\| \leq \phi$. The constraint $\|u(t)\|_2 \leq \mu$ is enforced at all times $t > 0$ if the LMIs*

$$\phi^2 I \leq X, \quad \begin{bmatrix} X & M_r{}^T \\ M_r & \mu^2 I \end{bmatrix} \geq 0$$

hold where $P = X^{-1}$ and $M_r = F_r X$.

The proofs of theorems 1-2 are based on the quadratic Lyapunov function of the form $V(x(t)) = x(t)^T P x(t)$ where $P = X^{-1}$. The proofs are given in [32]. The observer gains can be obtained solving the dual problem of the state feedback design, which approach will be followed in the remainder of the paper.

2.4 Robust control design

In a special class of the LPV system (3) the elements of parameter vector ρ are not measurable variables but represent variation of the system due to parametric uncertainties. The LMIs of Theorem 1 simplify to

$$\begin{aligned} &XA_r^T - M^T B_r^T + A_r X - B_r M < 0, \\ &XA_r^T - M^T B_r^T + A_s X \\ &- B_r M + XA_s^T - M^T B_s^T + A_s X - B_s M < 0 \end{aligned}$$

for $r < s \leq R$, except the pairs (r, s), such that $\forall \rho(t) : w_r(\rho(t))w_s(\rho(t)) = 0$, and where $M = FX$. The constant state feedback gain is derived as $F = MX^{-1}$. The proof can be derived using a quadratic Lyapunov function as shown in [14].

In a more general case when the parameter vector ρ can contain measurable elements in addition to the parameters that correspond to the uncertainty using constant controller gains leads to conservative results. The conservative nature of the control design can be avoided by a control structure in which the feedback and observer gains depend only on a subset of ρ. Let us group elements of the parameter vector ρ as follows

$$\rho(t) = \begin{bmatrix} \rho_{meas}(t) & \delta_{uc}(t) \end{bmatrix}^T \tag{11}$$

where ρ_{meas} contains the measurable elements and δ_{uc} contains the elements that correspond to the polytopic uncertainty. The dimension of ρ_{meas} and δ_{uc} is $N_{\rho_{meas}}$ and $N_{\delta_{uc}}$, respectively. The robust control structure can then be written as

$$\begin{aligned} \begin{bmatrix} \dot{\hat{x}}(t) \\ \hat{y}(t) \end{bmatrix} &= S(\rho(t)) \begin{bmatrix} \hat{x}(t) \\ u(t) \end{bmatrix} + \begin{bmatrix} K(\rho_{meas}(t)) \\ 0 \end{bmatrix} (y(t) - \hat{y}(t)), \\ u(t) &= -F(\rho_{meas}(t))\hat{x}(t). \end{aligned} \tag{12}$$

The TP type polytopic form of the state feedback gains and the observer gains in this case can be written as

$$\begin{aligned} F(\rho(t)) &= \mathcal{F} \overset{N_{\rho_{meas}}}{\underset{n=1}{\boxtimes}} w_n\left(\rho_n(t)\right), \\ K(\rho(t)) &= \mathcal{K} \overset{N_{\rho_{meas}}}{\underset{n=1}{\boxtimes}} w_n\left(\rho_n(t)\right). \end{aligned} \tag{13}$$

Core tensors $\mathcal{F}$ and $\mathcal{K}$ contain the state feedback gains $F_{i_1,\, i_2,\, ...,\, i_{N_{\rho_{meas}}}}$ and observer gains $K_{i_1,\, i_2,\, ...,\, i_{N_{\rho_{meas}}}}$. The state feedback gains can be obtained via the following theorems.

Theorem 3 Globally asymptotically stable robust control synthesis: *Consider the TP type polytopic model state feedback controller in the form of (12). The control structure is globally and asymptotically stable for the polytopic uncertain LPV model if matrices $X = X^T > 0$ and M_j satisfy the following inequalities*

$$\begin{aligned} &XA_r^T - M_j^T B_r^T + A_r X - B_r M_j < 0, \\ &XA_r^T - M_k^T B_r^T + A_s X - B_r M_k \\ &+ XA_s^T - M_j^T B_s^T + A_s X - B_s M_j < 0 \end{aligned}$$

for $r < s \leq R$, except the pairs (r, s), such that $\forall \rho(t) : w_r(\rho(t))w_s(\rho(t)) = 0$, for $j < k \leq R_{meas}$, except the pairs (j, k), such that $\forall \rho(t) : w_j(\rho(t))w_k(\rho(t)) = 0$, and where $M_j = F_j X$. The state feedback gains can be obtained as $F_j = M_j X^{-1}$.

Theorem 4 Robust constraint on the control value: *Assume that the upper bound of the initial condition is known and it is given by $\|x(0)\| \leq \phi$. The constraint $\|u(t)\|_2 \leq \mu$ is enforced at all times $t > 0$ if the LMIs*

$$\phi^2 I \leq X, \quad \begin{bmatrix} X & M_j^T \\ M_j & \mu^2 I \end{bmatrix} \geq 0$$

hold where $P = X^{-1}$ and $M_j = F_j X$.

The proofs of Theorems 3-4 use the Lyapunov function $V(x(t)) = x(t)^T P x(t)$ with $P = X^{-1}$ and are given in [14].

3 Uncertain Control Oriented Model of the FLEXOP Aircraft

The present section presents the main properties of the FLEXOP aircraft and the key ideas behind developing the uncertain control oriented model.

3.1 FLEXOP demonstrator aircraft

The FLEXOP aircraft has an aspect ratio of 20 and a wingspan of 7 m with a V-tail empennage [21]. The symmetric aeroelastic mode becomes unstable at 52 m/s airspeed and 50.2 rad/s frequency. The asymmetric flutter mode goes unstable at 55 m/s and 45.8 rad/s. Each wing has 4 control surfaces and custom made direct-drive actuators ensure sufficient bandwidth for active flutter suppression. In addition to the GPS and air data probe, the aircraft has inertial measurement units (IMUs) in the wings and at the center of gravity, see Figure 2.

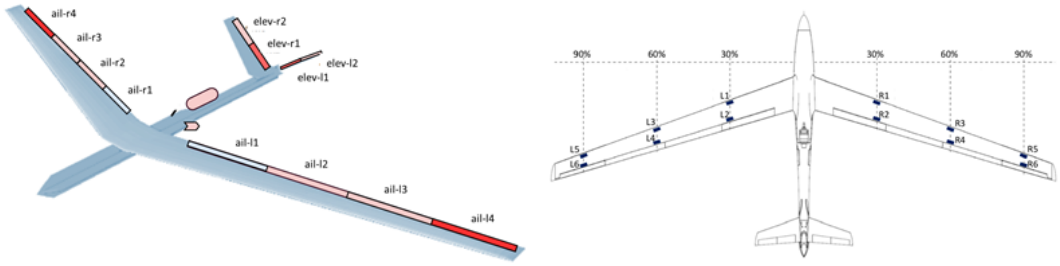

Figure 2: Control surfaces (top) and sensors (bottom).

3.2 High fidelity, uncertain nonlinear model

The ASE model of the FLEXOP aircraft is obtained by the subsystem approach, see Figure 3. The nominal, nonlinear ASE model of the FLEXOP aircraft consists of 12 rigid body states, 1040 aerodynamic lag states and 100 flexible mode states in addition to the states corresponding to the actuator dynamics, [39, 17]. The aerodynamic coefficients are assumed to be accurate and structural dynamics model to have parametric uncertainties with a significant effect on the flutter modes. Specifically, the first six modes have ±1% uncertainty in the natural frequency and ±10% in their damping.

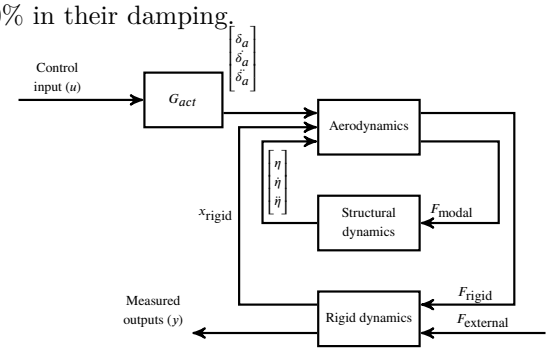

Figure 3: ASE subsystem interconnection.

3.3 Bottom-up modeling

Bottom-up modeling approach is pursued in order to obtain an ASE model of the FLEXOP aircraft that is of sufficiently low order for control design. The key idea is to reduce the subsystems first and then integrate them to form the ASE model [31, 17]. It is crucial to define the frequency range of interest in which high accuracy of the low order model is expected. The flutter frequencies are at 50.2 and 45.8 rad/s and adding a margin, the frequency range of interest is defined up to 100 rad/s. The ν-gap metric $\delta_\nu(\cdot,\cdot)$ between the high fidelity and low order models is used as the main measure of accuracy. It can take values between 0 and 1, 0 meaning that the two systems are identical [36]. The ν-gap metric is an LTI technique. Therefore, grid-based LPV models of the high-fidelity and reduced order ASE models are required. These LPV models are generated by trimming and linearizing the nonlinear models for straight and level flight at 26 points of the airspeed in the interval $[40, 65]$ m/s. The ν-gap metric is computed at each grid point and fixed frequencies for the $L4$, $R4$ ailerons and the vertical acceleration (a_z) sensors at the c.g. and at the 12 IMUs.

The structural dynamics model of the aircraft is

$$\mathcal{M}\ddot{\eta}(t) + \mathcal{C}\dot{\eta}(t) + \mathcal{K}\eta(t) = F_{\text{modal}}(t) \tag{14}$$

where η is the modal state, F_{modal} is the force acting on the structure in modal coordinates, $\mathcal{M}$, $\mathcal{C}$ and $\mathcal{K}$ are the modal mass, damping and stiffness matrices respectively. In order to keep the ν-gap between the high fidelity and the low order model low the first six structural modes and modes 19, 20, 21 are retained, the rest of the states are truncated.

The aerodynamic lag terms take the state-space form

$$\begin{aligned}\dot{x}_{\text{aero}}(t) &= \frac{2V_{\text{TAS}}(t)}{\bar{c}}A_{\text{lag}}x_{\text{aero}}(t) + B_{\text{lag}}\begin{bmatrix}\dot{x}_{\text{rigid}}(t)\\ \dot{\eta}(t)\\ \dot{\delta}_{\text{cs}}(t)\end{bmatrix}\\ y_{\text{aero}}(t) &= C_{\text{lag}}x_{\text{aero}}(t)\end{aligned} \tag{15}$$

where V_{TAS} is the true airspeed, x_{rigid} is the rigid body state, δ_{cs} is the control surface deflection and $\bar{c}$ is the reference chord. An LTI balancing transformation matrix T_{b} is computed for A_{lag}, B_{lag} and C_{lag}. The balanced

states with the smallest Hankel singular values are residualized. Retaining two lag states results in a low order model with acceptable accuracy. The bottom-up model therefore has 56 states. The ν-gap values and the pole migrations are given in Figure 4. The high fidelity model predicts flutter at 52 and 55 m/s at frequencies of 50.2 and 45.8 rad/s respectively while the low order model at 52 and 56.5 m/s at 50 and 46 rad/s respectively. Additional validation of the accuracy of the bottom-up model is given in [17].

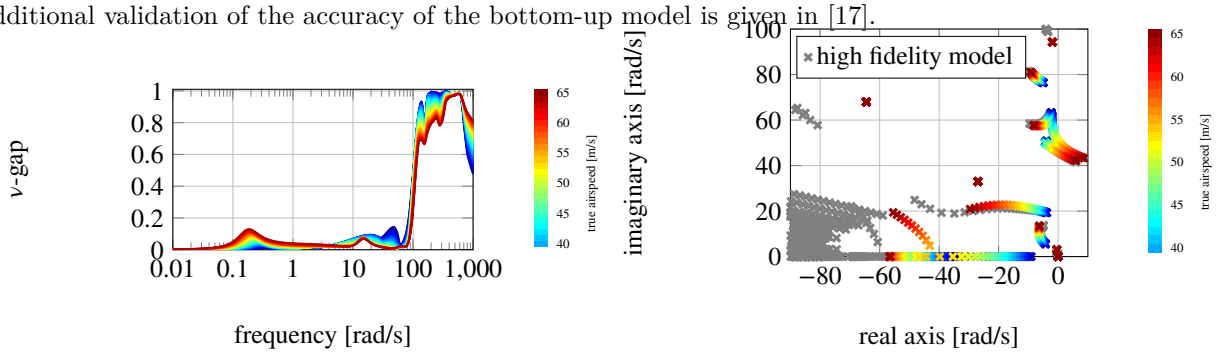

Figure 4: ν-gap values (top) and pole migration (bottom).

3.4 Control oriented uncertain TP models

Uncertain models can be developed by introducing uncertain parameters into the structural dynamics model. These uncertainties, denoted by $\delta_{\mathcal{K}}$ and $\delta_{\mathcal{C}}$, appear in the mass matrix $\mathcal{K}$ and in the damping matrix $\mathcal{C}$ of (14). The grid-based uncertain LPV model is obtained over a 3 dimensional grid. The grid consists of 26 equidistant points of the airspeed between 40 m/s and 65 m/s, 5 points of the natural frequency in the structural dynamics between $\pm 1\%$ of the nominal value, and 5 points of the damping in the structural dynamics between $\pm 10\%$ of the nominal value. The scheduling parameter ρ is defined as

$$\rho(t) = \begin{bmatrix} \rho_{V_{TAS}}(t) & \delta_{\mathcal{K}}(t) & \delta_{\mathcal{C}}(t) \end{bmatrix}^T \tag{16}$$

where $\rho_{V_{TAS}}$ is a measured parameter and $\delta_{\mathcal{K}}$ and $\delta_{\mathcal{C}}$ are unmeasured. The nominal and uncertain flutter modes of the control oriented LPV model are shown in Figure 5. The control oriented, uncertain TP model of the

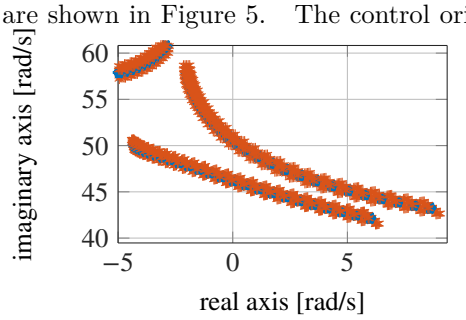

Figure 5: Flutter modes: nominal (blue), uncertain (red).

FLEXOP aircraft is obtained via TP model transformation. This control oriented model will serve as the basis for the flutter suppression control design. The first 5 singular values after TP model transformation in each dimension are the following

$$\begin{bmatrix} 2265597.18 \\ 65011.403 \\ 20.882 \\ 0.02596 \\ 0.0002635 \end{bmatrix}, \quad \begin{bmatrix} 2266526.615 \\ 3766.924 \\ 7.728e-05 \\ 1.114e-07 \\ 3.386e-09 \end{bmatrix}, \quad \begin{bmatrix} 2266529.745 \\ 9.142 \\ 2.989e-09 \\ 4.464e-11 \\ 1.221e-11 \end{bmatrix}.$$

The singular values related to the uncertainties have 2 dominant values in both dimensions. In case of the airspeed, it is possible to obtain a model with higher accuracy (HA) S_{HA} with $4 \times 2 \times 2 = 16$ vertex systems

by retaining the first four singular values. The model with lower complexity (LC) S_{LC} with $3 \times 2 \times 2 = 12$ vertex systems is obtained by retaining only the first three singular values.

$$\begin{aligned} S_{HA}(\rho) &= \sum_{i_1=1}^{4}\sum_{i_2=1}^{2}\sum_{i_3=1}^{2}\prod_{n=1}^{3} w_{n,i_n}(\rho_n) S_{i_1,\ldots,i_3} = \mathcal{S}_{HA} \overset{3}{\underset{n=1}{\boxtimes}} w_n(\rho_n) \\ S_{LC}(\rho) &= \sum_{i_1=1}^{3}\sum_{i_2=1}^{2}\sum_{i_3=1}^{2}\prod_{n=1}^{3} w_{n,i_n}(\rho_n) S_{i_1,\ldots,i_3} = \mathcal{S}_{LC} \overset{3}{\underset{n=1}{\boxtimes}} w_n(\rho_n) \end{aligned} . \tag{17}$$

TP model transformation based control design allows convex hull manipulation based control optimization. Therefore, CNO, IRNO and SNNN convex TP models are obtained for S_{HA} and S_{LC}. As a result, a set of models with different complexity and convex hulls are available for the control design. The weighting functions can be seen in Figures 6-7.

4 Flutter suppression control

4.1 Control design structure

The symmetrical and asymmetrical modes of the FLEXOP aircraft are decoupled, which enables independent control design for each flutter mode. The state feedback and observer gains depend only on $\rho_{meas} = \rho_{V_{TAS}}$ as:

$$\begin{aligned} F_{sym}(\rho(t)) &= \mathcal{F}_{sym} \overset{N_{\rho_{meas}}}{\underset{n=1}{\boxtimes}} w_n\left(\rho_{V_{TAS_n}}(t)\right), \\ K_{sym}(\rho(t)) &= \mathcal{K}_{sym} \overset{N_{\rho_{meas}}}{\underset{n=1}{\boxtimes}} w_n\left(\rho_{V_{TAS_n}}(t)\right), \\ F_{asym}(\rho(t)) &= \mathcal{F}_{asym} \overset{N_{\rho_{meas}}}{\underset{n=1}{\boxtimes}} w_n\left(\rho_{V_{TAS_n}}(t)\right), \\ K_{asym}(\rho(t)) &= \mathcal{K}_{asym} \overset{N_{\rho_{meas}}}{\underset{n=1}{\boxtimes}} w_n\left(\rho_{V_{TAS_n}}(t)\right). \end{aligned}$$

The symmetric model $S_{sym}(\rho(t))$ has input $u_{sym} = (L_4 + R_4)/2$ and output $y_{sym} = \begin{bmatrix}(a_{z,L3} + a_{z,R3})/2 & (a_{z,L6} + a_{z,R6})/2\end{bmatrix}^T$. The states are the vertical velocity w, pitch rate q, the symmetric modal coordinates, the lag states and the actuator states of the L_4 and R_4 control surfaces. The asymmetric model $S_{asym}(\rho(t))$ has inputs $u_{asym} = (L_4 - R_4)/2$ and outputs $y_{sym} = \begin{bmatrix}(a_{z,L3} - a_{z,R3})/2 & (a_{z,L6} - a_{z,R6})/2\end{bmatrix}^T$. The states are the horizontal velocity v, roll rate p, yaw rate r, the asymmetric modal coordinates, the lag states and actuator states of the L_4 and R_4 control surfaces. The observer based state feedback symmetric and asymmetric controllers can be connected with the high-fidelity FLEXOP model as shown in Figure 8. The control design is based on Theorems 3 and 4. Constraint $\phi = \|x(0)\| = 2$ of Theorem 4 is determined based on physical consideration and open loop simulations. The controller with lowest feasible μ ensures low control signal u and is considered optimal.

4.2 Influence of convex hull manipulation and model complexity

The paper focuses on CNO and IRNO type models for convex hull manipulation based optimization since the SNNN hull models do not yield feasible solutions. Interpolation between CNO and IRNO models is done as proposed in [28]:

$$w_{n_{INT}}(\rho_n) = (1-\lambda) w_{n_{CNO}}(\rho_n) + \lambda w_{n_{IRNO}}(\rho_n) \tag{18}$$

where $\lambda \in \begin{bmatrix}0 & 1\end{bmatrix}$. The interpolated core tensor $\mathcal{S}_{INT}$ is obtained by pseudo TP model transformation [6]. A set of six λ values are investigated for the lower complexity S_{LC} TP model. The achieved lower bounds of μ

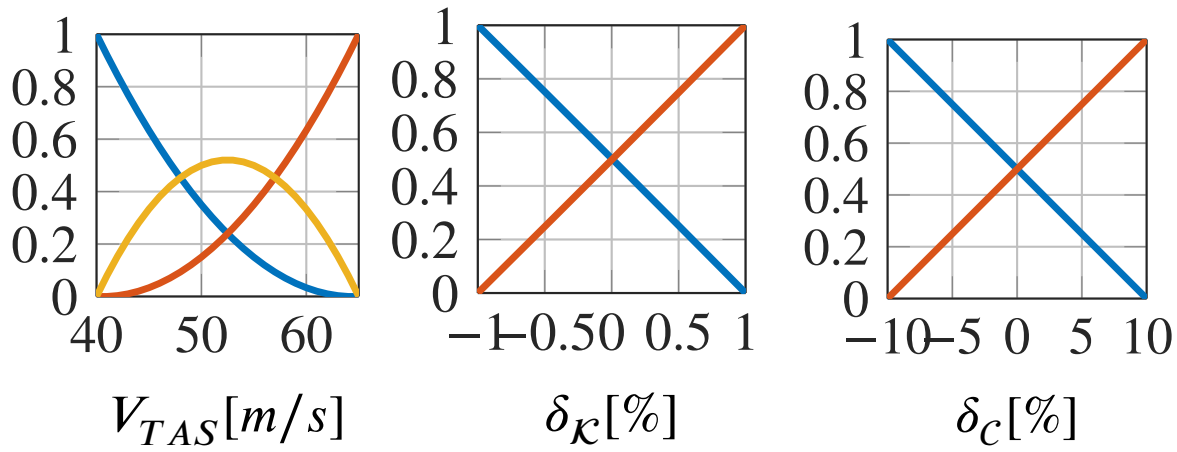

(a) CNO

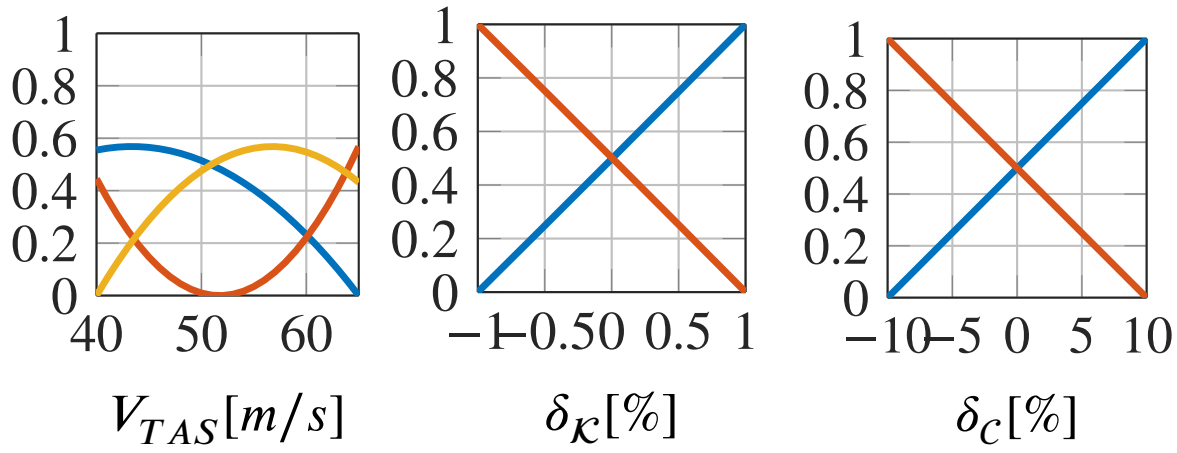

(b) IRNO

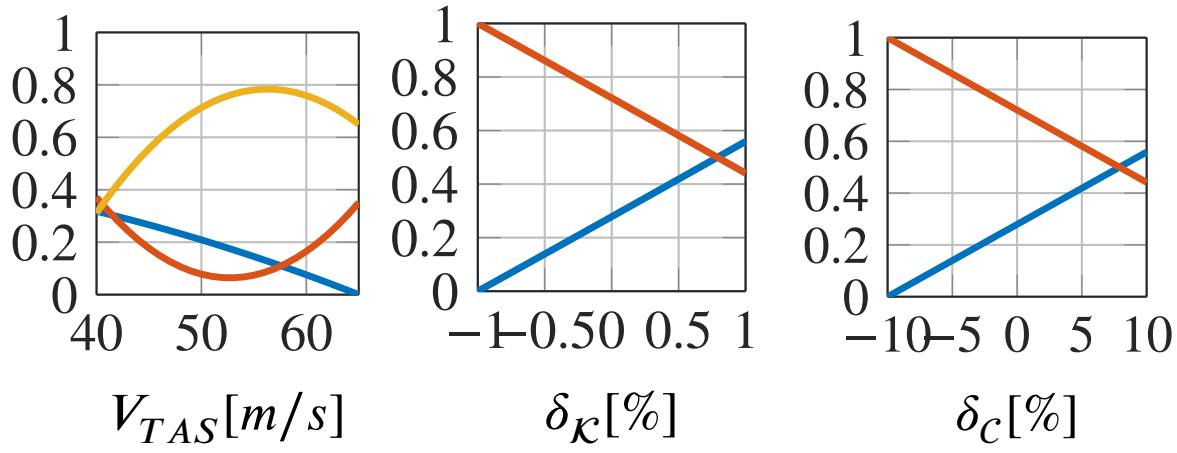

(c) SNNN

Figure 6: Weighting functions of S_{LC}.

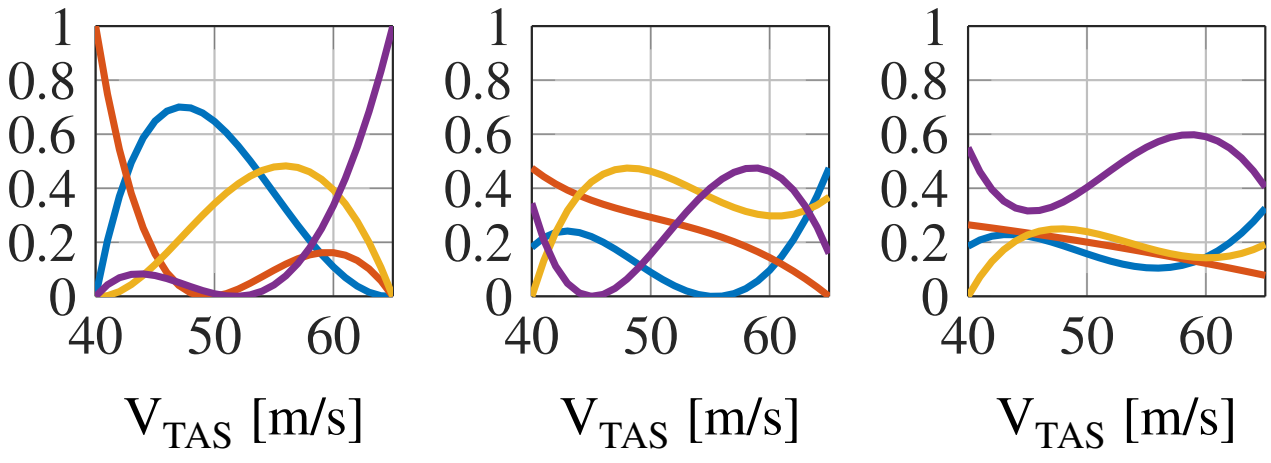

(a) CNO (b) IRNO (c) SNNN

Figure 7: Weighting functions of S_{HA}.

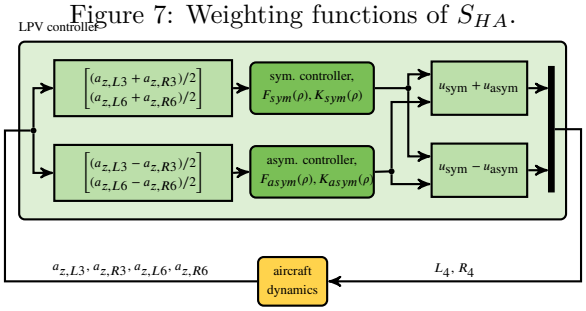

Figure 8: Control loop structure.

are given in Table 1. $\mu = \infty$ means that the LMIs of Theorem 3 are feasible, while the LMIs of Theorem 4 are not. This means that a stabilizing controller is obtained for all models, but constraint on the control values can only be enforced for lower λ values and the CNO type model leads to the best control performance. Note, that in some cases in the literature larger convex hulls lead to better observer performance [26, 27, 28]. The CNO type S_{AC} model is used to investigate the trade-off between accuracy and complexity of the model. Due to the increased complexity, the lower bound of μ increased compared to the CNO model of S_{LC}, as shown in Table 2. It can be concluded that the lower complexity, CNO type TP model of the FLEXOP aircraft leads to the best control performance. Extensive evaluations show that 3 vertex based TP type aeroelastic models have sufficiently high accuracy [29].

4.3 Frequency domain analysis

The resulting robust controller is connected to the high-fidelity, uncertain LPV model for the frequency domain analysis. The pole migrations of the open and closed loop systems are shown in Figure 9 for airspeed up to 61 m/s up to which the closed loop is stable. Both flutter modes are pushed to the left half plane and the remaining modes of the aircraft are not affected largely by the controller. The flutter-free envelope is therefore extended by approximately 11 %. The reason why the high fidelity model is stabilized up to 61 m/s instead of

λ	0	0.2	0.4	0.6	0.8	1
$\mu_{F_{sym}}$	32	36	48	391	∞	∞
$\mu_{F_{asym}}$	44	150	∞	∞	∞	∞
$\mu_{K_{sym}}$	2	2.3	2.5	2.8	2.96	2.9
$\mu_{K_{asym}}$	0.66	0.88	9.5	∞	∞	∞

Table 1: Lower bounds of μ as a function of λ for S_{LC}.

λ	$\mu_{F_{sym}}$	$\mu_{F_{asym}}$	$\mu_{K_{sym}}$	$\mu_{K_{asym}}$
0	∞	63	3.3	0.75

Table 2: Lower bounds of μ for the CNO model S_{HA}.

65 m/s is that the low order control oriented model does not capture the flutter modes perfectly. The accuracy can be improved by retaining more states in the model order reduction step. The fastest pole of the controller is at approximately $80 rad/s$, making it possible to be implemented on a digital computer. The Bode magnitude

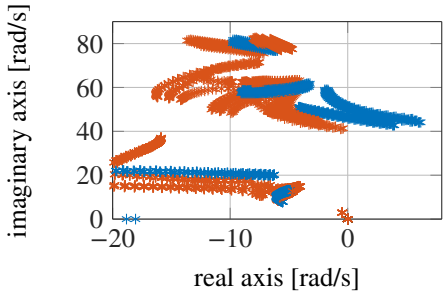

Figure 9: Pole migration of the uncertain, high-fidelity model; open loop (blue), closed loop (red).

plot of the resulting controller from the accelerometer $a_{z,L3}$ to the left aileron L_4 is shown in the left of Figure 10. The controller has peak gain around the flutter frequency which decreases at higher and lower frequencies, thus the rigid body dynamics and the unmodeled high frequency dynamics are not excited by the controller. The Bode magnitude of the open and closed loop systems from L_4 to $a_{z,L3}$ is shown in the right of Figure 10 for airspeed up to 61 ms showing that the flutter suppression increases the damping of the flutter modes. This figure also indicates that the designed controller acts mainly around the flutter frequency leaving the low and high frequency regions unaltered.

4.4 Time domain analysis

For time domain analysis the controller is connected with the uncertain, high-fidelity nonlinear ASE model of the FLEXOP aircraft as shown in Figure 8. The simulation starts with the aircraft trimmed for straight and level flight above the flutter speeds at 55 m/s. The speed is increased by adding a ramp signal on the throttle, see Figure 11. The control surfaces not involved in flutter suppression are kept at trim condition. Wind gusts are simulated by 2.5° doublets applied on the ailerons and elevators, exciting both the asymmetric and symmetric flutter modes. Sensor noise is added to the output signals. The computational time of the digital computer running the controller is accounted by 1 ms time delay. The response of the FLEXOP model with the natural frequency increased by 1% and the damping decreased by 10% are shown in Figure 11. Time domain simulations indicate that the FLEXOP aircraft remains stable up to approximately 61-62 m/s airspeed. The controller handled the time delay and sensor noise well, while the control commands are in the interval of ±2°, far from saturation. Note, that the effects of the time delay and sensor noise can also be explicitly accounted for in the control synthesis. Such approach should potentially increase the control performance.

Flutter suppression control design was in focus of several recent papers. [34] proposed robust control approach based on LTI model and synthesis. [30] provides an initial robust control for the FLEXOP aircraft, addressing the uncertainties in terms of LMIs. Such approach leads to high computational load of the LMI optimization. [37] proposed an LTI H_∞ method for the FLEXOP aircraft flutter suppression. [20] uses H_2 optimal blends of the input and output signals for aeroelastic mode control, also based on LTI models. An interesting future step can be to apply the input/output blending of [20] to the control structure presented in this paper.

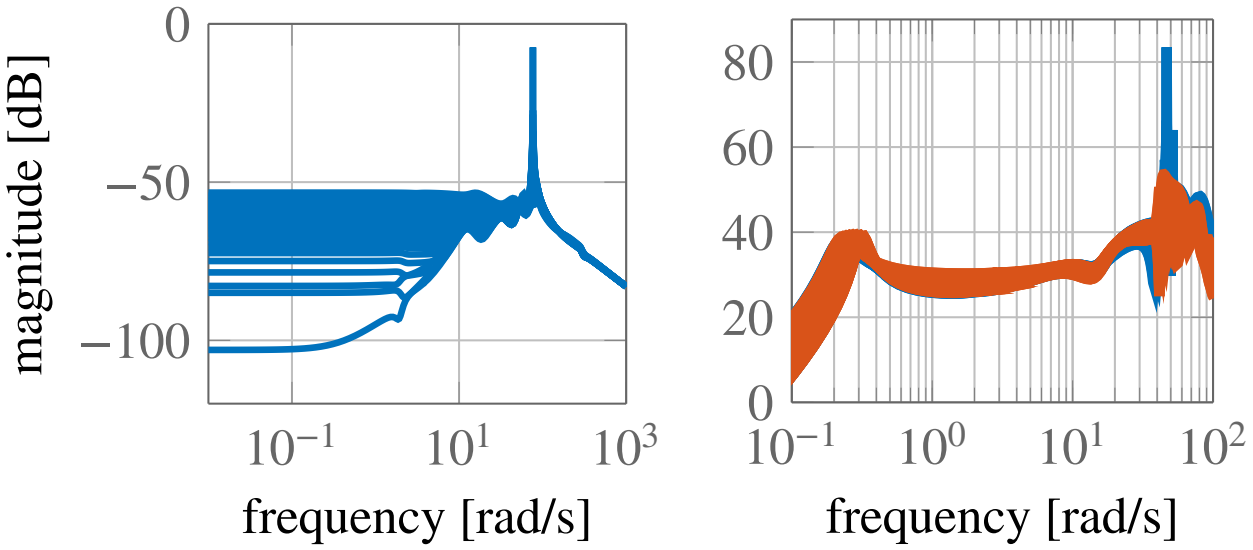

(a) LPV controller from $a_{z,L3}$ to L_4.

(b) Open and closed loops

Figure 10: Bode magnitude plots.

5 Conclusion

The paper presents a robust LPV flutter suppression design solution for the FLEXOP demonstrator aircraft. The uncertain low order model is developed by the "bottom-up" modeling approach and the control oriented LPV model is obtained via TP model transformation. The scheduling parameters are split into measured and uncertain parameters. Convex hull manipulation based optimization showed that for the FLEXOP aircraft tight convex hulls lead to the best performance and the lower complexity model results in better control performance. The resulting controller is analyzed with the high-fidelity uncertain LPV model and it is validated by numerical simulations using the high-fidelity, uncertain nonlinear model of the FLEXOP aircraft. The proposed control design extends the flutter-fee envelope from 52 m/s to approximately 61 ms. The control signals remain far from actuator saturation and the control performance is not degraded significantly due to computational time delay and sensor noise.

References

[1] P. Apkarian, P. Gahinet, and G. Becker, *Self-scheduled H∞ control of linear parameter-varying systems: a design example*, Automatica **31** (1995), no. 9, 1251–1261.

[2] P. Baranyi, *The generalized TP model transformation for T–S fuzzy model manipulation and generalized stability verification*, IEEE Transactions on Fuzzy Systems **22** (2014), no. 4, 934–948.

[3] P. Baranyi, *TP-model transformation-based-control design frameworks*, Springer, Cham, 2016.

[4] P. Baranyi, *Extension of the multi-TP model transformation to functions with different numbers of variables*, Complexity **2018** (2018), 1–9.

[5] P. Baranyi, *Extracting LPV and qLPV structures from state-space functions: A TP model transformation based framework*, IEEE Transactions on Fuzzy Systems **28** (2020), no. 3, 499–509.

[6] P. Baranyi, Y. Yam, and P. Varlaki, *Tensor Product Model Transformation in Polytopic Model-Based Control*, CRC Press, 2013.

[7] H. Bouzaouache, *Tensor product-based model transformation and optimal controller design for high order nonlinear singularly perturbed systems*, Asian Journal of Control **22** (2019), no. 1, 486–499.

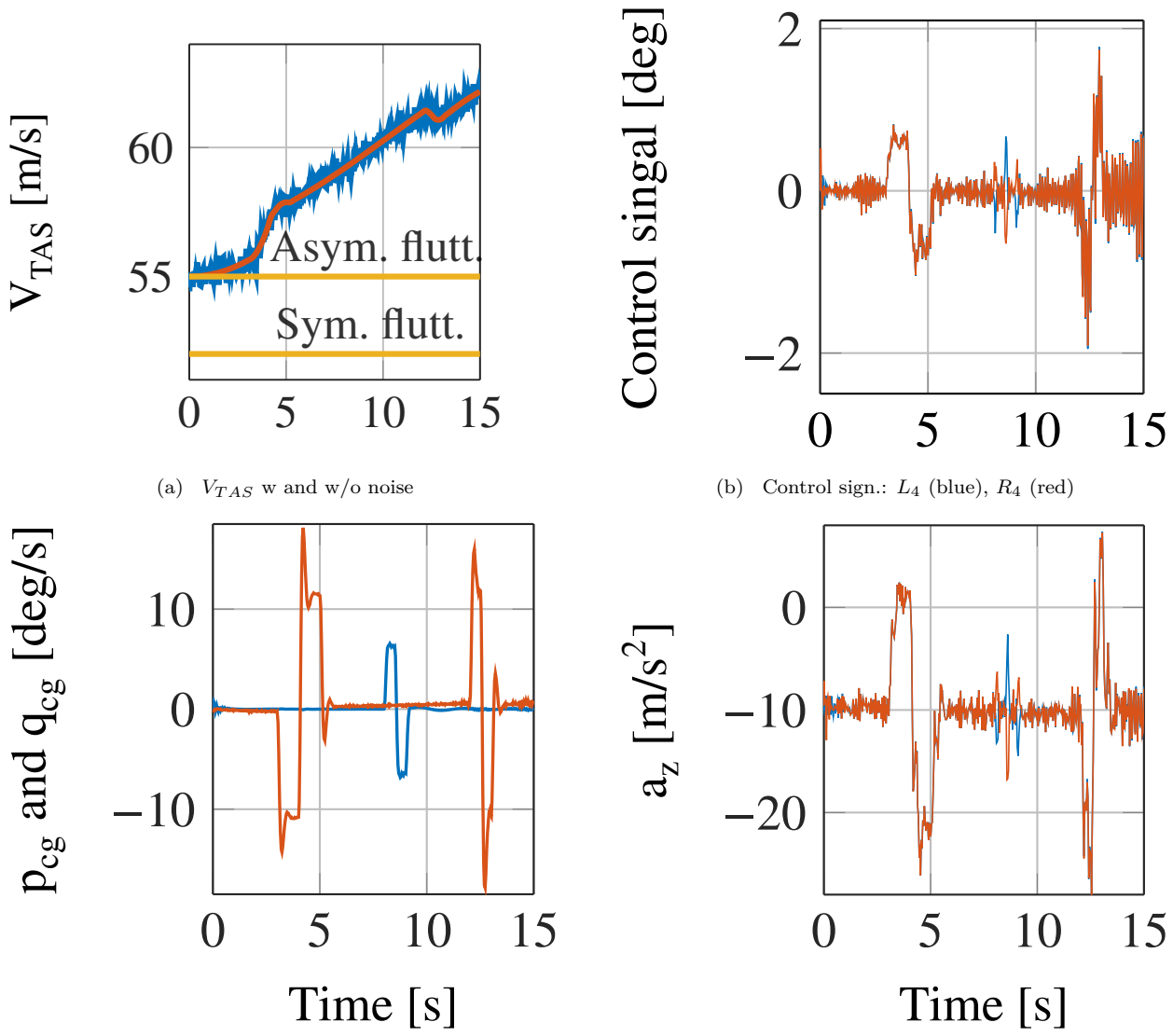

(a) V_{TAS} w and w/o noise

(b) Control sign.: L_4 (blue), R_4 (red)

(c) p_{cg} (blue), q_{cg} (red)

(d) $a_{z_{L6}}$ (blue), $a_{z_{R6}}$ (red)

Figure 11: Response of the FLEXOP aircraft.

[8] V. C. da Silva Campos, L. A. B. Tôrres, and R. M. Palhares, *Revisiting the TP model transformation: Interpolation and rule reduction*, Asian Journal of Control **17** (2014), no. 2, 392–401.

[9] L. De Lathauwer, B. De Moor, and J. Vandewalle, *A multilinear singular value decomposition*, SIAM Journal on Matrix Analysis and Applications **21** (2000), no. 4, 1253–1278.

[10] FLEXOP, *Flutter Free FLight Envelope eXpansion for ecOnomical Performance improvement (FLEXOP)*, H2020, Project ID: 636307, 2015-2018.

[11] FliPASED, *Flight Phase Adaptive Aero-Servo-Elastic Aircraft Design Methods (FliPASED)*, H2020, Project ID: 815058, 2019-2022.

[12] Y. Fung, *An introduction to the theory of aeroelasticity*, Edition Dover, 1969.

[13] A. Kotikalpudi, *Robust flutter analysis for aeroservoelastic systems*, Ph.D. thesis, University of Minnesota, 2017.

[14] J. Kuti, *Generalization of tensor product model based control analysis and synthesis*, Ph.D. thesis, Obuda University, 2017.

[15] T. Luspay et al., *Model reduction for LPV systems based on approximate modal decomposition*, International Journal for Numerical Methods in Engineering **113** (2017), no. 6, 891–909.

[16] T. Luspay et al., *Flight control design for a highly flexible flutter demonstrator*, *AIAA Scitech 2019 Forum*, AIAA, 2019–1817.

[17] Y. M. Meddaikar et al., *Aircraft aeroservoelastic modelling of the FLEXOP unmanned flying demonstrator*, *AIAA Scitech 2019 Forum*, AIAA, 2019–1815.

[18] PAAW, *Performance Adaptive Aeroelastic Wing Program*, Supported by NASA NRA "Lightweight Adaptive Aeroelastic Wing for Enhanced Perfromace Across the Flight Envelope", 2014-2019.

[19] A. Packard, *Gain scheduling via linear fractional transformations*, Systems & Control Letters **22** (1994), no. 2, 79–92.

[20] M. Pusch, *Aeroelastic mode control using h2-optimal blends for inputs and outputs*, *2018 AIAA Guidance, Navigation, and Control Conference*, American Institute of Aeronautics and Astronautics, 2018–0618.

[21] C. Roessler et al., *Aircraft design and testing of FLEXOP unmanned flying demonstrator to test load alleviation and flutter suppression of high aspect ratio flexible wings*, *AIAA Scitech 2019 Forum*, AIAA, 2019–1813.

[22] D. K. Schmidt, *Modern Flight Dynamics*, McGraw-Hill, 2012.

[23] D. K. Schmidt et al., *Flight-dynamics and flutter analysis and control of an MDAO-designed flying-wing research drone*, *AIAA Scitech 2019 Forum*, AIAA, 2019–1816.

[24] J. S. Shamma, *Analysis and design of gain scheduled control systems*, Ph.D. thesis, MIT, Cambridge, 1988.

[25] L. Szeidl and P. Várlaki, *HOSVD based canonical form for polytopic models of dynamic systems*, Journal of Advanced Computational Intelligence and Intelligent Informatics **13** (2009), no. 1, 52–60.

[26] A. Szollosi and P. Baranyi, *Influence of the Tensor Product model representation of qLPV models on the feasibility of Linear Matrix Inequality*, Asian Journal of Control **18** (2016), no. 4, 1328–1342.

[27] A. Szollosi and P. Baranyi, *Improved control performance of the 3-DoF aeroelastic wing section: a TP model based 2D parametric control performance optimization*, Asian Journal of Control **19** (2017), no. 2, 450–466.

[28] A. Szollosi and P. Baranyi, *Influence of the Tensor Product Model Representation of qLPV Models on the Feasibility of Linear Matrix Inequality based Stability Analysis*, Asian Journal of Control **20** (2017), no. 1, 531–547.

[29] B. Takarics, A. Szollosi, and B. Vanek, *Tensor product type polytopic LPV modeling of aeroelastic aircraft*, *2018 IEEE Aerospace Conference*, IEEE, 1–8.

[30] B. Takarics and B. Vanek, *Tensor product model-based robust flutter control design for the FLEXOP aircraft*, IFAC-PapersOnLine **52** (2019), no. 12, 134–139.

[31] B. Takarics et al., *Flight control oriented bottom-up nonlinear modeling of aeroelastic vehicles*, *2018 IEEE Aerospace Conference*, IEEE, 1–8.

[32] K. Tanaka and H. O. Wang, *Fuzzy Control Systems Design and Analysis: A Linear Matrix Inequality Approach*, 83–95 , John Wiley & Sons, Inc., 2001.

[33] J. Theis, H. Pfifer, and P. Seiler, *Robust control design for active flutter suppression*, *AIAA Science and Technology Forum and Exposition*, 2016–1751.

[34] J. Theis, H. Pfifer, and P. Seiler, *Robust control in flight: Active flutter suppression*, *AIAA Science and Technology Forum*, 2011–1751.

[35] J. Theis et al., *Modal matching for lpv model reduction of aeroservoelastic vehicles*, *AIAA Science and Technology Forum*, 2015–1686.

[36] G. Vinnicombe, *Measuring robustness of feedback systems*, Ph.D. thesis, Univ. Cambridge, Cambridge, 1993.

[37] S. Waitman and A. Marcos, *H∞ control design for active flutter suppression of flexible-wing unmanned aerial vehicle demonstrator*, Journal of Guidance, Control, and Dynamics **43** (2020), no. 4, 656–672.

[38] F. Wu, *Control of linear parameter varying systems*, Ph.D. thesis, Univ. California, Berkeley, 1995.

[39] M. Wuestenhagen et al., *Aeroservoelastic modeling and analysis of a highly flexible flutter demonstrator*, *2018 Atmospheric Flight Mechanics Conference*, AIAA, 2018–3150.

[40] Y. Yam and W. M. Lee, *Fuzzy controller/observer via grid point design and SVD consolidation*, *42nd IEEE CDC*, IEEE, 5526–5531.

Acknowledgments

Supported by the ÚNKP-20-5 New National Excellence Program of the Ministry for Innovation and Technology from the source of the National Research, Development and Innovation Fund.

The research leading to these results is part of the FLiPASED project. This project has received funding from the European Unions Horizon 2020 research and innovation programme under grant agreement No 815058.

This paper was supported by the János Bolyai Research Scholarship of the Hungarian Academy of Sciences.

The research reported in this paper and carried out at the Budapest University of Technology and Economics was supported by the "TKP2020, Institutional Excellence Program" of the National Research Development and Innovation Office in the field of Artificial Intelligence (BME IE-MI-FM TKP2020).

Author Biography

Béla Takarics received his M.S. and a Ph.D. degree in mechanical engineering from the Budapest University of Technology and Economics, Budapest, Hungary, in 2007 and 2012 respectively. He is currently a senior research fellow at the Systems and Control Lab (SCL) of the Research Institute for Computer Science and Control (SZTAKI). His research interests include multi-objective and integral quadratic constraints based robust control of LPV systems, modeling and active control of aeroservoelastic vehicles.

Bálint Vanek received his M.S. degree in mechanical engineering from the Budapest University of Technology and Economics, Budapest, Hungary, in 2003 and a Ph.D. in aerospace engineering from the University of Minnesota, Minnesota, USA in 2008. He is currently a senior research fellow and leader of the Aerospace Guidance, Navigation, and Control Group at the Systems and Control Lab (SCL) of the Research Institute for Computer Science and Control (SZTAKI). His research interests include flight control, fault detection, unmanned aerial vehicles (UAVs), inertial and satellite navigation systems.